HHS Public Access

Author manuscript

Inorg Chem. Author manuscript; available in PMC 2023 February 07.

Published in final edited form as:

Inorg Chem. 2022 February 07; 61(5): 2662–2668. doi:10.1021/acs.inorgchem.1c03790.

Involvement of a Formally Copper(III) Nitrite Complex in Proton-Coupled Electron Transfer and Nitration of Phenols

Caitlin J. Bouchey,

Department of Chemistry, Washington University in St. Louis, St. Louis, Missouri 63130, United States; Department of Chemistry, University of Minnesota, Minneapolis, Minnesota 55455, United States

William B. Tolman

Department of Chemistry, Washington University in St. Louis, St. Louis, Missouri 63130, United States

Abstract

A unique high-valent copper nitrite species, $LCuNO_2$, was accessed via the reversible one-electron oxidation of [M][$LCuNO_2$] (M = NBu_4^+ or PPN^+). The complex $LCuNO_2$ reacts with 2,4,6-tri-*tert*-butylphenol via a typical proton-coupled electron transfer (PCET) to yield LCuTHF and the 2,4,6-tri-*tert*-butylphenoxyl radical. The reaction between $LCuNO_2$ and 2,4-di-*tert*-butylphenol was more complicated. It yielded two products: the coupled bisphenol product expected from a H-atom abstraction and 2,4-di-*tert*-butyl-6-nitrophenol, the product of an unusual anaerobic nitration. Various mechanisms for the latter transformation were considered.

Graphical Abstract

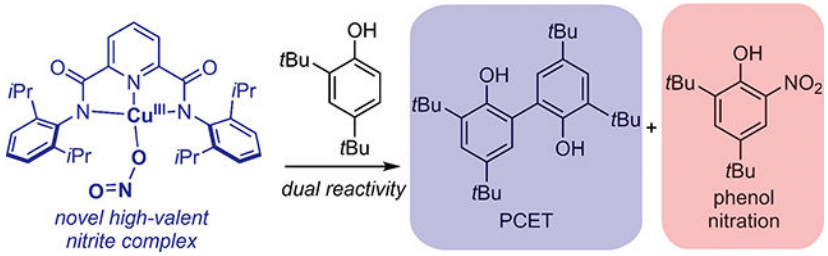

Corresponding Author William B. Tolman – wbtolman@wustl.edu.

The authors declare no competing financial interest.

■ ASSOCIATED CONTENT

Supporting Information

The Supporting Information is available free of charge at https://pubs.acs.org/doi/10.1021/acs.inorgchem.1c03790.

Experimental details, UV–vis and EPR spectral data, cyclic voltammetry data, oxidation of Cu^{II} via UV–vis, resonance Raman spectral data, UV–vis spectral reactivity traces, EPR and UV–vis spectral product analysis, reactivity plot, ^1H NMR spectral product analysis, and an alternative nitration mechanism (PDF)

Accession Codes

CCDC 2125948 contains the supplementary crystallographic data for this paper. These data can be obtained free of charge via www.ccdc.cam.ac.uk/data_request/cif, or by emailing data_request@ccdc.cam.ac.uk, or by contacting The Cambridge Crystallographic Data Centre, 12 Union Road, Cambridge CB2 1EZ, UK; fax: +44 1223 336033.

■ INTRODUCTION

Copper nitrite complexes have been studied extensively as models for the active sites of copper-containing nitrite reductases (CuNIRs),[1–25] key enzymes in global denitrification and mammalian and plant signaling pathways.[26] These model complexes contain Cu^{I} or Cu^{II}, often in coordination geometries relevant to the CuNIR active site, and they typically reduce NO_2^- to NO, a reaction also performed by the enzymes. It has been proposed for CuNIRs that one-electron reduction of NO_2^- to NO involves an initial proton transfer facilitated by neighboring amino acid residues.[27–31] Inspired by this notion, recent work has probed the ability of copper(II) nitrite complexes to perform proton-coupled electron transfer (PCET).[10,19] Notably, PCET was invoked in the reaction of a copper(II) nitrite complex with 2,4-di-*tert*-butylphenol (DTBP) that underwent subsequent nitration, an unusual anaerobic transformation.[19] Such a process is relevant to tyrosine nitration, which normally occurs via an attack by peroxynitrite.[32–34]

Considering that higher-oxidation-state species generally exhibit enhanced PCET reactivity,[35–38] we sought to prepare a complex with a $[CuNO_2]^{2+}$ core (formally containing Cu^{III}) that would represent a rare example of a high-valent metal nitrite species.[39–41] Specifically, previous success in using the hindered dianionic ligand bis(2,6-diisopropylphenylcarboxamido)-pyridine (L^{2-}) to prepare reactive complexes with cores $[CuX]^{2+}$ (X = OR,[42–47] SR,[48] OOR,[49] O_2CR,[50,51] F, Cl, and Br[52]) led us to target $LCuNO_2$. Herein, we describe the successful generation and spectroscopic characterization of this novel high-valent metal nitrite species, as well as preliminary studies of PCET reactivity with phenolic substrates that result in an unusual anaerobic nitration.

■ RESULTS AND DISCUSSION

Synthesis and Characterization of $[M][LCuNO_2]$ ($M = NBu_4^+$ or PPN^+).

The addition of the corresponding nitrite salt $[M][NO_2]$ to LCu(MeCN) (MeCN = acetonitrile) in tetrahydrofuran (THF) resulted in the formation of copper(II) complexes $[M][LCuNO_2]$ ($M = NBu_4^+$ or PPN^+), which were isolated as powder blue solids and characterized by elemental analysis, UV–vis and electron paramagnetic resonance (EPR) spectroscopy, and X-ray crystallography for $M = PPN^+$ (Scheme 1). The X-ray structure of $[PPN][LCuNO_2]$ shows nitrite bound strongly to the Cu ion through one O atom [Cu1–O3 = 1.9667(13) Å] with an additional weak interaction through the second O atom [Cu1–O4 = 2.4622(14) Å; Figure 1]. This binding geometry is similar to that observed for carboxylate ligands in the series $[NBu_4][LCu(O_2CR)]$,[50,51] and the N–O bond distances are comparable to those in other complexes containing $Cu^{II}(\eta^1\text{-ONO})$ cores.[3,13–15,17,19,24,51,53–59] The Cu ion adopts a square-planar geometry ($\tau_4 = 0.16$),[60] and the Cu1–N1, Cu1–N2, and Cu1–N3 bond lengths are similar to those in the previously reported $[LCuX]^-$ complexes.[42,44,46–52]

The X-band EPR spectra for $[M][LCuNO_2]$ ($M = NBu_4^+$ or PPN^+) in THF at 30 K are nearly identical and exhibit typical signals for $S = {}^1/_2$ square-planar copper(II) complexes (Figures 2 and S1). Spectral parameters were estimated by simulation, with the best match to the 17-line experimental superhyperfine pattern resulting when only three N atoms were included (Table S1). From these results and the similarity of the spectrum to those of other

$[LCuX]^-$ complexes,[42,44,46–52] we conclude that little spin density is present on the nitrite N atom and that the superhyperfine coupling arises from interactions with the N atoms of L^{2-}. The UV–vis spectra for $[M][LCuNO_2]$ (M = NBu_4^+ or PPN^+) in THF show typical d–d transitions ($\lambda \sim 586$ nm; $\varepsilon \sim 480$ M^{-1} cm^{-1}; Figure S2). Cyclic voltammetry for $[NBu_4][LCuNO_2]$ in THF (0.3 M $[NBu_4][PF_6]$) revealed a pseudoreversible wave with $E_{1/2}$ = +180 mV versus ferrocene/ferrocenium (Fc/Fc^+; linear plot of i_{pa} vs $\nu^{1/2}$; Figure S3). This oxidation potential is similar to those measured for the $[LCu(O_2CR)]^{-/0}$ series (range = 150–298 mV)[51] and 347 mV higher than that for $[LCuOH]^{-/0}$,[47] all which track inversely with the basicity of the anionic "X" ligands (greater basicity, lower potential; Table S2).

Synthesis and Characterization of $LCuNO_2$.

The addition of 1 equiv of acetylferrocenium tetrakis(3,5-bis-(trifluoromethyl)phenyl)borate ($[AcFc][BArF_{24}]$) to a solution of $[NBu_4][LCuNO_2]$ in THF at −80 °C resulted in the immediate development of a deep Prussian blue color and the appearance of intense features at 478 nm (ε = 5350 $M^{-1}cm^{-1}$), 655 nm (ε = 9170 M^{-1} cm^{-1}), and 816 nm (ε = 7180 M^{-1} cm^{-1}) in the UV–vis spectrum (Figure 3a). Variation of the amount of $[AcFc]^+$ between 0.2 and 1.8 equiv showed the attainment of maximum absorbance for the new features when 1 equiv of $[AcFc]^+$ was added (Figures 3b and S4). Also, the addition of 1 equiv of decamethylferrocene (Fc*) bleached the solution to yield the spectrum of $[LCuNO_2]^-$, a process that could be repeated (2 times; Figure S5). Taken together, the evidence supports reversible one-electron oxidation of $[NBu_4][LCuNO_2]$.

The new UV–vis features that appear upon oxidation of $[NBu_4][LCuNO_2]$ are similar to those seen for other LCuX complexes and bear particular resemblance to those found for the $LCuO_2CR$ series.[51] These features were assigned using time-dependent density functional theory to ligand-to-metal charge transfer (LMCT) involving *N*-aryl $\pi \rightarrow$ Cu d and *N*-amide $\pi \rightarrow$ Cu d transitions.[50] Consistent with these assignments, the energy of these transitions is inversely proportional to the electron-withdrawing characteristics of the carboxylate ligand. Thus, for example, $LCuO_2CC_6F_5$ with the most electron-withdrawing carboxylate and the lowest carboxylic acid aqueous pK_a of 1.48[61] yields the most electrophilic Cu ion and the lowest-energy feature at 866 nm, whereas $LCuO_2CCH_3$ with its absorption feature at 809 nm has the least electrophilic Cu ion in the series with a carboxylic acid aqueous pK_a of 4.8.[51] The lowest-energy peak for the product of one-electron oxidation of $[NBu_4][LCuNO_2]$ has λ_{max} = 816 nm, intermediate in the $LCuO_2CR$ series, consistent with a nitrous acid aqueous pK_a of 3.16, and in line with an analogous LMCT assignment.[62] Finally, a peak at 634 cm^{-1} was observed in the resonance Raman spectrum of $LCuNO_2$ (λ_{ex} = 660 nm), which we assign as ν(Cu–O) based on nearly identical peaks present in previously measured spectra for LCuX with X = O-based ligands (Figure S6).[47,49] Taken together, the UV–vis and resonance Raman spectra and titration/stoichiometry/reversibility data support formation of $LCuNO_2$ upon one-electron oxidation of $[NBu_4][LCuNO_2]$.

PCET Reactivity.

Treatment of $LCuNO_2$ with 2,4,6-tri-*tert*-butylphenol (TTBP; 50 equiv) in THF at −80 °C led to decay of the absorptions associated with $LCuNO_2$. This decay was monitored over ~40 min, and a global fit of the decay spectra to a second-order reaction model using

ReactLab Kinetics[63] yielded a k_2 of 1(1) × 10^{-1} M^{-1} s^{-1}. The UV–vis spectrum of the product solution (Figure S7) indicated formation of the 2,4,6-tri-*tert*-butylphenoxyl radical (characteristic peaks around 400 and 660 nm)[64,65] and LCu(THF) (d–d transition at 570 nm).[50] The radical was also identified by EPR spectroscopy, and from integration, a yield of 61% was determined (Figure S8). In a separate experiment designed to detect possible coproduct NO, a solution of TTBP (50 equiv) was added to a solution of $LCuNO_2$ at −40 °C and allowed to warm to room temperature in the presence of a solution of CoTPP (TPP = 5,10,15,20-tetraphenyl-21*H*,23*H*-porphine).[20,40,66,67] Subsequent analysis of the latter solution by UV–vis spectroscopy revealed the formation of (NO)CoTPP in an amount corresponding to ~15% yield of NO from the PCET reaction (Figure S9). We presume that HNO_2 also forms in the PCET reaction but decays via unidentified processes, which might also lead to NO. An alternative PCET pathway (analogous to the one previously identified in a reaction of the Cu^{II}-NO_2 complex)[19] would involve the initial formation of NO and $LCu^{III}OH$, but the latter would be expected to react further with TTBP and generate an additional 1 equiv of the phenoxyl radical (Scheme S1). The observed low yield of the radical and the low yield of NO argue against this pathway being the dominant H-atom-transfer step.[68,69]

The rate constant found for the reaction of TTBP with $LCuNO_2$ is similar to that for the reaction with $LCuO_2CC_6H_4(Cl)$ under the same conditions [k_2 = 3(1) × 10^{-1} M^{-1} s^{-1}],[50] but it is ~100 times smaller than that for the reaction with LCuOH [k_2 = 2(1) × 10^1 M^{-1} s^{-1}].[50] These rate constants are in line with thermodynamic considerations, particularly the $E_{1/2}$ and pk_a values. Thus, the $[LCuNO_2]^{-/0}$ $E_{1/2}$ of 180 mV versus Fc/Fc^+ and the pK_a of HNO_2 of 3.16[62] fall close to the corresponding $E_{1/2}$ and carboxylic acid pK_a values for the series $[LCuO_2CR]^{-/0}$, and the former $E_{1/2}$ values correlate with the log k_2 values for the reaction with TTBP (Figure S10).[51] These relationships support similar driving forces for the PCET reactions. Likewise, the greater basicity of LCuOH that results in the formation of a stronger O–H bond underlies its faster PCET reactions.[43]

Nitration Reactivity.

UV–vis monitoring of the reactions between $LCuNO_2$ and varying amounts of DTBP (1–60 equiv) in THF at −40 °C resulted in $t_{1/2}$ values of 613, 318, 252, and 176 s in the presence of 1, 20, 40, and 60 equiv of substrate, respectively (Figure S11). While the trend in the $t_{1/2}$ values indicates a dependence of the rate on the DTBP concentration, the decay data could not be fit to simple kinetic models (i.e., pseudo first order; Figure S11c,f,i,l). These findings suggest that a more complicated reaction occurs with DTBP compared to TTBP. Product analysis was performed in an attempt to understand the results from the kinetic experiments. A peak at 570 nm in the final UV–vis spectrum suggests formation of LCu(THF). To identify the organic products, reactions were performed on a larger scale (2.67 mM) at −40 °C in THF using 0.5 or 1 equiv of DTBP for 2 h or 10 equiv of DTBP for 1 h, and the residues were analyzed by ^{1}H NMR spectroscopy (Figures S12–S14). Two products were identified: the coupled bisphenol product, 3,3′,5,5′-tetra-*tert*-butyl-[1,1′-biphenyl]-2,2′-diol, and 2,4-di-*tert*-butyl-6-nitrophenol (Scheme 2). The yields of bisphenol and 2,4-di-*tert*-butyl-6-nitrophenol and the amount of unreacted DTBP varied with differing equivalents of DTBP (Table 1). The data show that the yield of nitrated product and the

conversion of substrate increase in the reactions with fewer equivalents of DTBP used. We interpret these results (greater nitration when $LCuNO_2$ is in excess) to indicate that nitration involves multiple equivalents of $LCuNO_2$.

The product 2,4-di-*tert*-butyl-6-nitrophenol could be formed from the reaction between $LCuNO_2$ and DTBP via multiple possible mechanisms. $LCuNO_2$ could abstract a H atom from DTBP, resulting in a $[LCuHNO_2]$ adduct (which presumably decays to LCuTHF and HNO_2) and the phenoxyl radical of DTBP, which could react with another 1 equiv of $LCuNO_2$ in a "rebound" type of reaction to form LCuTHF and a nitrated phenol product (Scheme 3, path A). There is precedence to support the "rebound" pathway given that LCuF was reported to functionalize substrates via H-atom abstraction and radical capture, or "rebound".[52] Conversely, multiple pathways where free NO_2 is liberated are possible (Scheme 3), and free NO_2 has been studied for its oxidation and nitration chemistry with DTBP.[70] If $LCuNO_2$ does disproportionate into LCuTHF and free NO_2, then this is an unusual transformation of mildly oxidizing nitrite to NO_2. The results of the stoichiometry experiments are taken as evidence for Scheme 3, with path A being the predominant nitration mechanism, because the dependence of the nitrated product yield on the stoichiometry of $LCuNO_2$ suggests that limiting consumption of $LCuNO_2$ by PCET favors nitration.

$LCuNO_2$ could be involved in generation of the phenoxyl radical of DTBP via a nucleophilic attack of the phenol on the nitrite ligand of $LCuNO_2$, as previously seen for a Cu^{II}-NO_2 compound (Scheme S2).[66,71] The products of the nucleophilic attack would be O-nitrosated DTBP and $LCu^{III}OH$, which would react with another 1 equiv of DTBP to form bisphenol. The O-nitrosated DTBP would then release NO and the phenoxyl radical of DTBP, which could then combine to form 2,4-di-*tert*-butyl-6-nitrophenol.[71] The stoichiometry experiments do not support this nitration mechanism because it does not use more than 1 equiv of $LCuNO_2$ to nitrate the phenol. However, we cannot rule out nucleophilic attack of the phenol on $LCuNO_2$ to form the phenoxyl radical of DTBP, which then could react with another 1 equiv of $LCuNO_2$ via the "rebound" mechanism.

Alternatively, 2 equiv of the $[LCuHNO_2]$ adduct could functionalize DTBP directly, resulting in the nitrated phenol product of DTBP (Scheme 3, path B). This mechanism is consistent with the stoichiometry experiments, and there is literature precedence for the involvement of a nitrous acid adduct, $[CoHNO_2]^{2+}$,[72] nitrating DTBP. However, we view this mechanism unlikely for $[LCuHNO_2]$ because one of the products would be an unprecedented $\{CuNO\}^{10}$ complex.

Yet another pathway to generate 2,4-di-*tert*-butyl-6-nitrophenol from $LCuNO_2$ and DTBP would involve one-electron oxidation of DTBP by $LCuNO_2$, with the resulting cation-radical phenol species reacting with free nitrite, as proposed for the protonated cryptand-capped tripodal Cu^{II}-NO_2 compound.[19,73] We rule this pathway out because the reported E_{ox} value of DTBP is 1.03 V versus Fc/Fc^+ (converted from 1.43 V vs SCE),[74] which is about 800 mV higher than the $E_{1/2}$ value found for the $[LCuNO_2]^{-/0}$ couple. As discussed for the protonated cryptand-capped tripodal Cu^{II}-NO_2 compound, phenol nitration typically occurs via O_2-dependent pathways through metal peroxynitrite species. The reactions of the

compounds $LCuNO_2$ and the protonated cryptand-capped tripodal Cu^{II}-NO_2 species are two recent examples of phenol nitration that occur through uncommon anaerobic pathways.[19]

■ CONCLUSIONS

The copper(II) nitrite starting materials [M][$LCuNO_2$] (M = NBu_4^+ or PPN^+) were prepared and characterized by UV–vis and EPR spectroscopy, CHN analysis, and X-ray crystallography. Electrochemical and chemical oxidations of $[LCuNO_2]^-$ revealed a reversible one-electron oxidation to an intriguing $[CuNO_2]^{2+}$ core, and $LCuNO_2$ was characterized at low temperatures by UV–vis and resonance Raman spectroscopies. To our knowledge, this complex is a unique example of a high-valent copper nitrite complex. The reaction between $LCuNO_2$ and TTBP revealed that $LCuNO_2$ can abstract H atoms from O–H substrates at rates comparable to those in $LCuO_2CR$ complexes.[51] Interestingly, the reaction between $LCuNO_2$ and DTBP yielded not only the expected PCET product but the *ortho*-nitrated phenol as well. Although there are multiple possible mechanisms that could result in the nitrated phenol, detection of the nitrated product indicates that $LCuNO_2$ (or a derivative) can functionalize substrates, a type of transformation that has only been demonstrated by X = halides for LCuX complexes.[52]

Supplementary Material

Refer to Web version on PubMed Central for supplementary material.

■ ACKNOWLEDGMENTS

We thank the National Institutes of Health (Grant GM47365) for financial support and Dr. Dimitar Shopov for collecting EPR data. X-ray diffraction data were collected using a diffractometer acquired through NSF-MRI Award CHE-1827756.

■ REFERENCES

(1). Kujime M; Izumi C; Tomura M; Hada M; Fujii H Effect of a Tridentate Ligand on the Structure, Electronic Structure, and Reactivity of the Copper(I) Nitrite Complex: Role of the Conserved Three-Histidine Ligand Environment of the Type-2 Copper Site in Copper-Containing Nitrite Reductases. J. Am. Chem. Soc. 2008, 130 (19), 6088–6098. [PubMed: 18412340]

(2). Kujime M; Fujii H Spectroscopic Characterization of Reaction Intermediates in a Model for Copper Nitrite Reductase. Angew. Chemie - Int. Ed. 2006, 45 (7), 1089–1092.

(3). Scarpellini M; Neves A; Castellano EE; De Almeida Neves EF; Franco DW A Nitrite Reductase with a Polyimidazole Tripodal Ligand. Polyhedron 2004, 23 (4), 511–518.

(4). Merkle AC; Lehnert NStructural Model for Oxidized Type II Copper. Binding and Activation of Nitrite and Nitric Oxide by Copper Nitrite Reductase and Corresponding Model Complexes. Dalt. Trans. 2012, 41 (12), 3355–3368.

(5). Monzani E; Koolhaas GJAA; Spandre A; Leggieri E; Casella L; Gullotti M; Nardin G; Randaccio L; Fontani M; Zanello P; et al. Binding of Nitrite and Its Reductive Activation to Nitric Oxide at Biomimetic Copper Centers. J. Biol. Inorg. Chem. 2000, 5 (2), 251–261. [PubMed: 10819470]

(6). Halfen JA; Tolman WB Synthetic Model of the Substrate Adduct to the Reduced Active Site of Copper Nitrite Reductase. J. Am. Chem. Soc. 1994, 116 (12), 5475–5476.

(7). Beretta M; Bouwman E; Casella L; Douziech B; Driessen WL; Gutierrez-Soto L; Monzani E; Reedijk J Copper Complexes of a New Tridentate Imidazole-Containing Ligand: Spectroscopy, Structures and Nitrite Reductase Reactivity: The Molecular Structures of [Cu(Biap)(NO2)2] and [Cu(Biap)Br2]. Inorg. Chim. Acta 2000, 310 (1), 41–50.

(8). Tolman WB A Model for the Substrate Adduct of Copper Nitrite Reductase and Its Conversion to a Novel Tetrahedral Copper(II) Triflate Complex. Inorg. Chem. 1991, 30 (26), 4877.

(9). Hsu SCN; Chang Y; Chuang W; Chen H; Lin I; Chiang MY; Kao C; Chen H Copper(I) Nitro Complex with an Anionic [HB(3,5-Me2Pz)3]- Ligand: A Synthetic Model for the Copper Nitrite Reductase Active Site. Inorg. Chem. 2012, 51 (17), 9297–9308. [PubMed: 22905707]

(10). Cioncoloni G; Roger I; Wheatley PS; Wilson C; Morris RE; Sproules S; Symes MD Proton-Coupled Electron Transfer Enhances the Electrocatalytic Reduction of Nitrite to NO in a Bioinspired Copper Complex. ACS Catal. 2018, 8 (6), 5070–5084.

(11). Kumar M; Dixon NA; Merkle AC; Zeller M; Lehnert N; Papish ET Hydrotris(Triazolyl)Borate Complexes as Functional Models for Cu Nitrite Reductase: The Electronic Influence of Distal Nitrogens. Inorg. Chem. 2012, 51 (13), 7004–7006. [PubMed: 22671968]

(12). Monzani E; Koolhaas GJAA; Spandre A; Leggieri E; Casella L; Gullotti M; Nardin G; Randaccio L; Fontani M; Zanello P; et al. Binding of Nitrite and Its Reductive Activation to Nitric Oxide at Biomimetic Copper Centers. J. Biol. Inorg. Chem. 2000, 5 (2), 251–261. [PubMed: 10819470]

(13). Casella L; Carugo O; Gullotti M; Doldi S; Frassoni M Synthesis, Structure, and Reactivity of Model Complexes of Copper Nitrite Reductase. Inorg. Chem. 1996, 35 (5), 1101–1113. [PubMed: 11666296]

(14). Maji RC; Barman SK; Roy S; Chatterjee SK; Bowles FL; Olmstead MM; Patra AK Copper Complexes Relevant to the Catalytic Cycle of Copper Nitrite Reductase: Electrochemical Detection of NO(g) Evolution and Flipping of NO2 Binding Mode upon CuII → CuI Reduction. Inorg. Chem. 2013, 52 (19), 11084–11095. [PubMed: 24066957]

(15). Arnold PJ; Davies SC; Durrant MC; Griffiths DV; Hughes DL; Sharpe PC Copper(II) Nitrite Complexes of Tripodal Ligands Derived from 1,1,1-Tris(2-Pyridyl)Methylamine. Inorg. Chim. Acta 2003, 348, 143–149.

(16). Lehnert N; Cornelissen U; Neese F; Ono T; Noguchi Y; Okamoto KI; Fujisawa K Synthesis and Spectroscopic Characterization of Copper(II)-Nitrito Complexes with Hydrotris(Pyrazolyl)-Borate and Related Coligands. Inorg. Chem. 2007, 46 (10), 3916–3933. [PubMed: 17447754]

(17). Chandra Maji R; Mishra S; Bhandari A; Singh R; Olmstead MM; Patra AK A Copper(II) Nitrite That Exhibits Change of Nitrite Binding Mode and Formation of Copper(II) Nitrosyl Prior to Nitric Oxide Evolution. Inorg. Chem. 2018, 57 (3), 1550. [PubMed: 29355312]

(18). Chen CS; Yeh WY Coordination of NO2- Ligand to Cu(I) Ion in an O, O-Bidentate Fashion That Evolves NO Gas upon Protonation: A Model Reaction Relevant to the Denitrification Process. Chem. Commun. 2010, 46 (18), 3098–3100.

(19). Mondal A; Reddy KP; Bertke JA; Kundu S Phenol Reduces Nitrite to NO at Copper(II): Role of a Proton-Responsive Outer Coordination Sphere in Phenol Oxidation. J. Am. Chem. Soc. 2020, 142 (4), 1726–1730. [PubMed: 31910624]

(20). Moore CM; Szymczak NK Nitrite Reduction by Copper through Ligand-Mediated Proton and Electron Transfer. Chem. Sci. 2015, 6, 3373. [PubMed: 28706701]

(21). Halfen JA; Mahapatra S; Wilkinson EC; Gengenbach AJ; Young VG; Que L Jr; Tolman WB<au/> Synthetic Modeling of Nitrite Binding and Activation by Reduced Copper Proteins. Characterization of Copper(I)-Nitrite Complexes That Evolve Nitric Oxide. J. Am. Chem. Soc. 1996, 118 (4), 763–776.

(22). Halfen JA; Mahapatra S; Olmstead MM; Tolman WB Synthetic Analogues of Nitrite Adducts of Copper Proteins: Characterization and Interconversion of Dicopper(I, I) and -(I, II) Complexes Bridged Only by NO2-. J. Am. Chem. Soc. 1994, 116 (5), 2173.

(23). Chuang WJ; Lin IJ; Chen HY; Chang YL; Hsu SCN Characterization of a New Copper(I)-Nitrito Complex That Evolves Nitric Oxide. Inorg. Chem. 2010, 49 (12), 5377–5384. [PubMed: 20481524]

(24). Yokoyama H; Yamaguchi K; Sugimoto M; Suzuki S CuI and CuII Complexes Containing Nitrite and Tridentate Aromatic Amine Ligand as Models for the Substrate-Binding Type-2 Cu Site of Nitrite Reductase. Eur. J. Inorg. Chem. 2005, 2 (8), 1435–1441.

(25). Chang YL; Lin YF; Chuang WJ; Kao CL; Narwane M; Chen HY; Chiang MY; Hsu SCN Structure and Nitrite Reduction Reactivity Study of Bio-Inspired Copper(I)-Nitro Complexes in

Steric and Electronic Considerations of Tridentate Nitrogen Ligands. Dalt. Trans. 2018, 47 (15), 5335–5341.

(26). Maia LB; Moura JJG How Biology Handles Nitrite. Chem. Rev. 2014, 114 (10), 5273–5357. [PubMed: 24694090]

(27). Zhao Y; Lukoyanov DA; Toropov YV; Wu K; Shapleigh JP; Scholes CP Catalytic Function and Local Proton Structure at the Type 2 Copper of Nitrite Reductase: The Correlation of Enzymatic PH Dependence, Conserved Residues, and Proton Hyperfine Structure. Biochemistry 2002, 41 (23), 7464–7474. [PubMed: 12044180]

(28). Suzuki S; Kataoka K; Yamaguchi K Metal Coordination and Mechanism of Multicopper Nitrite Reductase. Acc. Chem. Res. 2000, 33 (10), 728–735. [PubMed: 11041837]

(29). Fukuda Y; Tse KM; Nakane T; Nakatsu T; Suzuki M; Sugahara M; Inoue S; Masuda T; Yumoto F; Matsugaki N; et al. Redox-Coupled Proton Transfer Mechanism in Nitrite Reductase Revealed by Femtosecond Crystallography. Proc. Natl. Acad. Sci. U. S. A. 2016, 113 (15), 2928–2933. [PubMed: 26929369]

(30). Kataoka K; Furusawa H; Takagi K; Yamaguchi K; Suzuki S Functional Analysis of Conserved Aspartate and Histidine Residues Located around the Type 2 Copper Site of Copper-Containing Nitrite Reductase. J. Biochem. 2000, 127 (2), 345–350. [PubMed: 10731703]

(31). Ghosh S; Dey A; Sun Y; Scholes CP; Solomon EI Spectroscopic and Computational Studies of Nitrite Reductase: Proton Induced Electron Transfer and Backbonding Contributions to Reactivity. J. Am. Chem. Soc. 2009, 131 (1), 277–288. [PubMed: 19053185]

(32). Radi R Nitric Oxide, Oxidants, and Protein Tyrosine Nitration. Proc. Natl. Acad. Sci. U. S. A. 2004, 101 (12), 4003–4008. [PubMed: 15020765]

(33). Ferrer-Sueta G; Campolo N; Trujillo M; Bartesaghi S; Carballal S; Romero N; Alvarez B; Radi R Biochemistry of Peroxynitrite and Protein Tyrosine Nitration. Chem. Rev. 2018, 118 (3), 1338–1408. [PubMed: 29400454]

(34). Qiao L; Lu Y; Liu B; Girault HH Copper-Catalyzed Tyrosine Nitration. J. Am. Chem. Soc. 2011, 133 (49), 19823–19831. [PubMed: 22046951]

(35). Warren JJ; Tronic TA; Mayer JM Thermochemistry of Proton-Coupled Electron Transfer Reagents and its Implications. Chem. Rev. 2010, 110, 6961–7001. [PubMed: 20925411]

(36). Mayer JM Proton-coupled electron transfer: a reaction chemist's view. Annu. Rev. Phys. Chem. 2004, 55, 363–90. [PubMed: 15117257]

(37). Yosca TH; Rittle J; Krest CM; Onderko EL; Silakov A; Calixto JC; Behan RK; Green MT Iron(IV)hydroxide pKa and the Role of Thiolate Ligation in C-H Bond Activation by Cytochrome P450. Science 2013, 342, 825–829. [PubMed: 24233717]

(38). A counterexample where greater PCET reactivity for a lower oxidation state complex is observed: (a) Borovik AS Role of metal-oxo complexes in the cleavage of C-H bonds. Chem. Soc. Rev. 2011, 40, 1870–1874. [PubMed: 21365079] (b)Parsell T; Yang M; Borovik A C-H Bond Cleavage with Reductants: Re-Investigating the Reactivity of Monomeric Mn III/IV-Oxo Complexes and the Role of Oxo Ligand Basicity. J. Am. Chem. Soc. 2009, 131, 2762–2763. [PubMed: 19196005]

(39). Lee NF; Malone J; Jeddi H; Kwong KW; Zhang R Visible-Light Photolysis of Corrole-Manganese(IV) Nitrites to Generate Corrole-Manganese(V)-Oxo Complexes. Inorg. Chem. Commun. 2017, 82, 27–30.

(40). Shi K; Mathivathanan L; Boudalis AK; Turek P; Chakraborty I; Raptis RG Nitrite Reduction by Trinuclear Copper Pyrazolate Complexes: An Example of a Catalytic, Synthetic Polynuclear NO Releasing System. Inorg. Chem. 2019, 58 (11), 7537–7544. [PubMed: 31091082]

(41). Dulong F; Pouessel J; Thuéry P; Berthet JC; Ephritikhine M; Cantat T Nitrite Complexes of Uranium and Thorium. Chem. Commun. 2013, 49 (24), 2412–2414.

(42). Donoghue PJ; Tehranchi J; Cramer CJ; Sarangi R; Solomon EI; Tolman WB Rapid C-H Bond Activation by a Monocopper(III)-Hydroxide Complex. J. Am. Chem. Soc. 2011, 133 (44), 17602–17605. [PubMed: 22004091]

(43). Dhar D; Tolman WB Hydrogen Atom Abstraction from Hydrocarbons by a Copper(III)-Hydroxide Complex. J. Am. Chem. Soc. 2015, 137 (3), 1322–1329. [PubMed: 25581555]

(44). Dhar D; Yee GM; Spaeth AD; Boyce DW; Zhang H; Dereli B; Cramer CJ; Tolman WB Perturbing the Copper(III)-Hydroxide Unit through Ligand Structural Variation. J. Am. Chem. Soc. 2016, 138 (1), 356–368. [PubMed: 26693733]

(45). Dhar D; Yee GM; Markle TF; Mayer JM; Tolman WB Reactivity of the Copper(III)-Hydroxide Unit with Phenols. Chem. Sci. 2017, 8 (2), 1075–1085. [PubMed: 28572905]

(46). Dhar D; Yee GM; Tolman WB Effects of Charged Ligand Substituents on the Properties of the Formally Copper(III)-Hydroxide ([CuOH] 2+) Unit. Inorg. Chem. 2018, 57 (16), 9794–9806. [PubMed: 30070473]

(47). Krishnan VM; Shopov DY; Bouchey CJ; Bailey WD; Parveen R; Vlaisavljevich B; Tolman WB Structural Characterization of the [CuOR]2+Core. J. Am. Chem. Soc. 2021, 143 (9), 3295–3299. [PubMed: 33621089]

(48). Wu W; De Hont JT; Parveen R; Vlaisavljevich B; Tolman WB Sulfur-Containing Analogues of the Reactive [CuOH] 2+ Core. Inorg. Chem. 2021, 60 (7), 5217–5223. [PubMed: 33733755]

(49). Neisen BD; Gagnon NL; Dhar D; Spaeth AD; Tolman WB Formally Copper(III)-Alkylperoxo Complexes as Models of Possible Intermediates in Monooxygenase Enzymes. J. Am. Chem. Soc. 2017, 139 (30), 10220–10223. [PubMed: 28722408]

(50). Mandal M; Elwell CE; Bouchey CJ; Zerk TJ; Tolman WB; Cramer CJ Mechanisms for Hydrogen-Atom Abstraction by Mononuclear Copper(III) Cores: Hydrogen-Atom Transfer or Concerted Proton-Coupled Electron Transfer? J. Am. Chem. Soc. 2019, 141 (43), 17236–17244. [PubMed: 31617707]

(51). Elwell CE; Mandal M; Bouchey CJ; Que L; Cramer CJ; Tolman WB Carboxylate Structural Effects on the Properties and Proton-Coupled Electron Transfer Reactivity of [CuO2CR]2+ Cores. Inorg. Chem. 2019, 58 (23), 15872–15879. [PubMed: 31710477]

(52). Bower JK; Cypcar AD; Henriquez B; Stieber SCE; Zhang SC(Sp3)-H Fluorination with a Copper(II)/(III) Redox Couple. J. Am. Chem. Soc. 2020, 142 (18), 8514–8521. [PubMed: 32275410]

(53). Allman R; Kremer S; Kucharzcyk D The Crystal Structure and EPR G-Tensors of [Cuterpy(ONO)OH2]NO2 H20. Inorg. Chim. Acta 1984, 85, L19–L21.

(54). Maria S; Chattopadhyay T; Ananya S; Kundu S Reduction of Nitrite to NO at a Mononuclear Copper(II)-Phenolate Site. Inorg. Chim. Acta 2020, 506, 119515.

(55). Hill SJ; Hubberstey P; Li W Bis (Diimine)Nitritocopper(Ll) Cations: Crystal and Molecular Structures of [Cu(Phen)2(ONO)] BF4 H20 and [Cu(Bipy)2(ONO)]HSO4 {phen = 1,10 Phenanthroline, Bipy = 2,2'-Bipyridine}. Polyhedron 1997, 16 (14), 2447–2453.

(56). Kumar Lal T; Richardson JF; Mashuta MS; Buchanan RM; Mukherjee R Synthesis, X-Ray Structure and Properties of a New Nitrite-Bound Copper(II) Complex with 2-(3,5-Dimethylpyrazol-1-Ylmethyl)Pyridine in a CuN4(O) Coordination. Polyhedron 1997, 16 (24), 4331–4336.

(57). Komeda N; Nagao H; Kushi Y; Adachi G; Suzuki M; Uehara A; Tanaka K Molecular Structure of Nitro- and Nitrito-Copper Complexes as Reaction Intermediates in Electrochemical Reduction of Nitrite to Dinitrogen Oxide. Bull. Chem. Soc. Jpn. 1995, 68, 581–589.

(58). Sarkar B; Konar S; Gomez-Garcia CJ; Ghosh A Rare Example of U-Nitrito-1-k-2O, O':2KO Coordinating Mode in Copper(II) Nitrite Complexes with Monoanionic Tridentate Schiff-Base Ligands: Structure, Magnetic, and Electrochemical Properties. Inorg. Chem. 2008, 47 (24), 11611–11619. [PubMed: 18998624]

(59). Jiang F; Conry RR; Bubacco L; Tyeklar Z; Jacobson RR; Karlin KD; Peisach J Crystal Structure and Electron Spin Echo Envelope Modulation Study of [Cu(II)(TEPA)(NO2)]PF6 (TEPA = Tris[2-(2-Pyridyl)Ethyl]Amine): A Model for the Purported Structure of the Nitrite Derivative of Hemocyanin. J. Am. Chem. Soc. 1993, 115 (6), 2093–2102.

(60). Yang L; Powell DR; Houser RP Structural Variation in Copper(i) Complexes with Pyridylmethylamide Ligands: Structural Analysis with a New Four-Coordinate Geometry Index, T4. J. Chem. Soc. Dalt. Trans. 2007, No. 9, 955–964.

(61). Prakash GKS; Hu J Pentafluorobenzoic Acid. Encyclopedia of Reagents for Organic Synthesis; John Wiley and Sons: Chichester, U.K., 2006.

(62). Da Silva G; Kennedy EM; Dlugogorski BZ Ab Initio Procedure for Aqueous-Phase PKa Calculation: The Acidity of Nitrous Acid. J. Phys. Chem. A 2006, 110 (39), 11371–11376. [PubMed: 17004748]

(63). Maeder M; King P Reactlab; Jplus Consulting Pty Ltd.: East Freemantle, Australia, 2009.

(64). Manner VW; Markle TF; Freudenthal JH; Roth JP; Mayer JM The First Crystal Structure of a Monomeric Phenoxyl Radical: 2,4,6-Tri-Tert-Butylphenoxyl Radical. Chem. Commun. 2008, 246 (2), 256–258.

(65). Porter TR; Capitao D; Kaminsky W; Qian Z; Mayer JM Synthesis, Radical Reactivity, and Thermochemistry of Monomeric Cu(II) Alkoxide Complexes Relevant to Cu/Radical Alcohol Oxidation Catalysis. Inorg. Chem. 2016, 55 (11), 5467–5475. [PubMed: 27171230]

(66). Kundu S; Kim WY; Bertke JA; Warren TH Copper(II) Activation of Nitrite: Nitrosation of Nucleophiles and Generation of NO by Thiols. J. Am. Chem. Soc. 2017, 139 (3), 1045–1048. [PubMed: 27936678]

(67). Sakhaei Z; Kundu S; Donnelly JM; Bertke JA; Kim WY; Warren TH Nitric Oxide Release via Oxygen Atom Transfer from Nitrite at Copper(II). Chem. Commun. 2017, 53 (3), 549–552.

(68). Park JY; Lee YN Solubility and Decomposition Kinetics of Nitrous Acid in Aqueous Solution. J. Phys. Chem. 1988, 92 (22), 6294–6302.

(69). Chen X; Fuller ME; Franklin Goldsmith C Decomposition Kinetics for HONO and HNO2. React. Chem. Eng. 2019, 4 (2), 323–333.

(70). Astolfi P; Panagiotaki M; Greci L New Insights into the Reactivity of Nitrogen Dioxide with Substituted Phenols: A Solvent Effect. Eur. J. Org. Chem. 2005, 2005 (14), 3052–3059.

(71). Sakhaei Z; Kundu S; Bertke JA; Warren TH Nitrite-Phenol-NO Crosstalk: Phenol Oxidation and NO Generation from Nitrite at Copper(II) Sites. ChemRxiv 2019. DOI: 10.26434/chemrxiv.11341544.v1.

(72). Puthiyaveetil Yoosaf MA; Ghosh S; Narayan Y; Yadav M; Sahoo SC; Kumar P Finding a New Pathway for Acid-Induced Nitrite Reduction Reaction: Formation of Nitric Oxide with Hydrogen Peroxide. Dalt. Trans. 2019, 48 (37), 13916–13920.

(73). We performed reactions between $LCuNO_2$ and DTBP (THF, −40 C) in the presence of excess nitrite (10 equiv) and observed almost instantaneous decay of the complex, and organic product analysis revealed no PCET product or nitrated phenol from these reactions. We currently do not understand why excess nitrite facilitates the decay of $LCuNO_2$.

(74). Osako T; Ohkubo K; Taki M; Tachi Y; Fukuzumi S; Itoh S Oxidation Mechanism of Phenols by Dicopper-Dioxygen (Cu2/O 2) Complexes. J. Am. Chem. Soc. 2003, 125 (36), 11027–11033. [PubMed: 12952484]

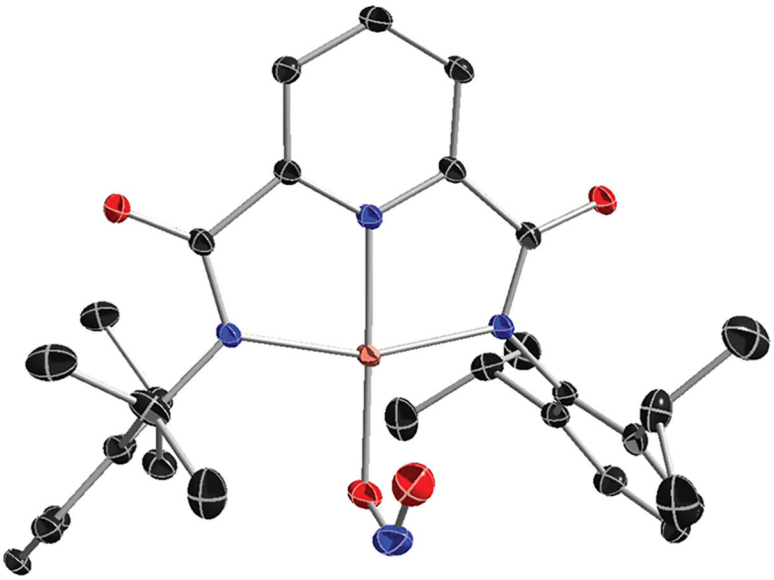

Figure 1.

X-ray crystal structure of [PPN][LCuNO$_2$] with the PPN cation and H atoms omitted for clarity. All non-H atoms are shown as 30% thermal ellipsoids. Selected bond distances (Å) and angles (deg): Cu1–O3, 1.9667(13); Cu1–O4, 2.4622(14); Cu1–N1, 1.9987(13); Cu1–N2, 1.9242(14); Cu1–N3, 1.9985(13); N1–Cu1–N3, 160.25(6); N1–Cu1–N2, 80.26(5); N2–Cu1–N3, 80.48(6); N2–Cu1–O3, 178.01(6).

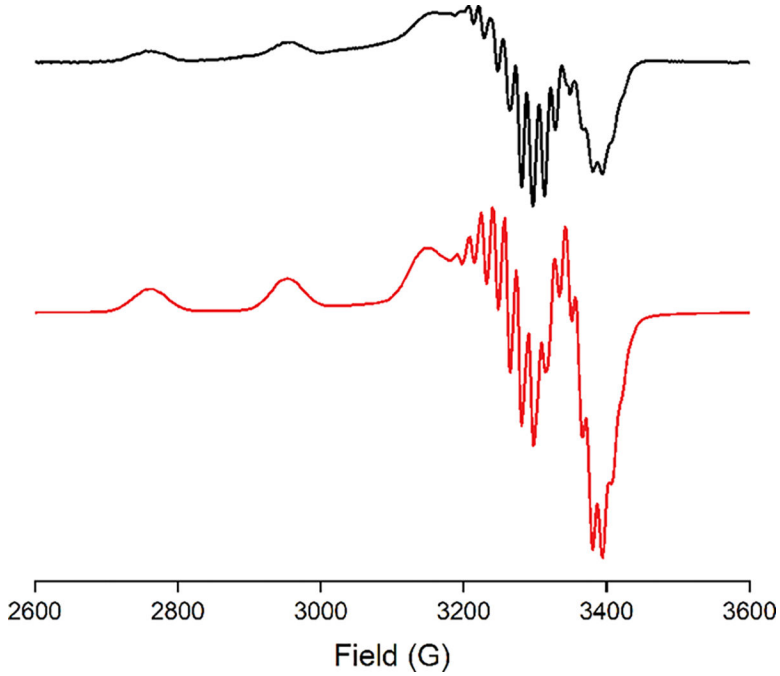

Figure 2.

X-band EPR spectrum of $[NBu_4][LCuNO_2]$ in THF (black, experimental; red, simulation). Parameters: temperature 30 K; microwave frequency 9.38 GHz; microwave power 0.0002 mW; modulation amplitude 9.8 G; modulation frequency 100 kHz. Parameters from the simulation are listed in Table S1.

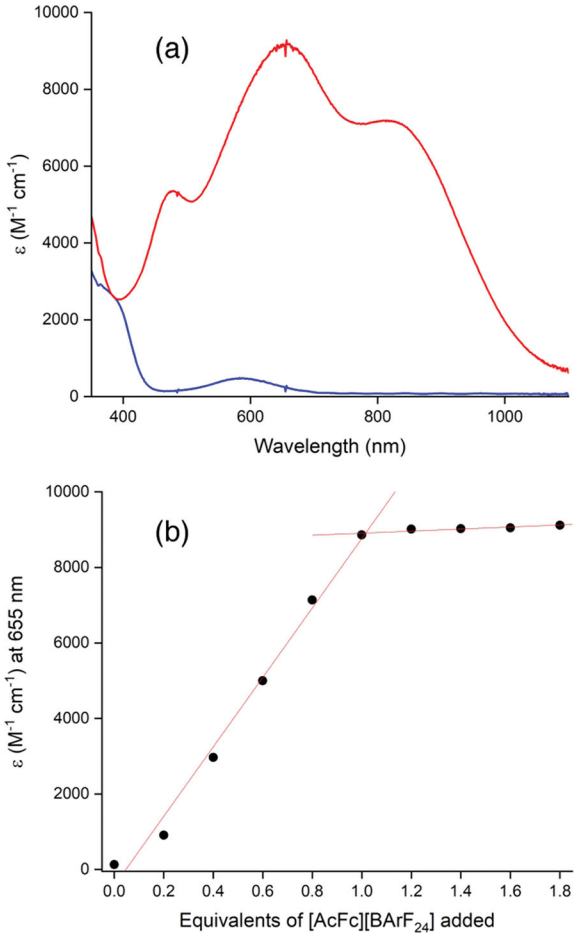

Figure 3.

(a) Overlay of UV–vis spectra of $[NBu_4][LCuNO_2]$ (blue) and the species generated upon the addition of 1 equiv of $[AcFc][BArF_{24}]$ to $[NBu_4][LCuNO_2]$ (red). Conditions: −80 °C in THF. (b) Plot of corresponding molar absorptivity values at λ = 655 nm versus equivalents of $[AcFc][BArF_{24}]$ added to $[NBu_4][LCuNO_2]$ at −80 °C in THF.

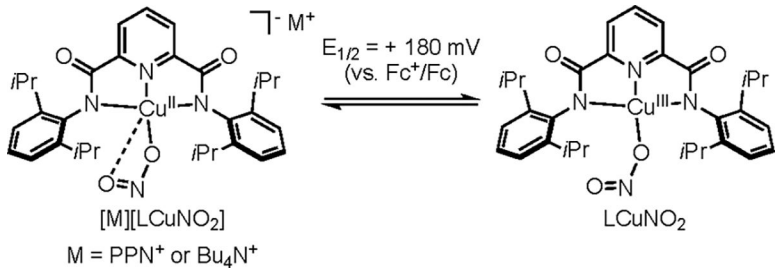

Scheme 1. Copper Complexes Discussed in This Work, with Formal Oxidation States Indicated

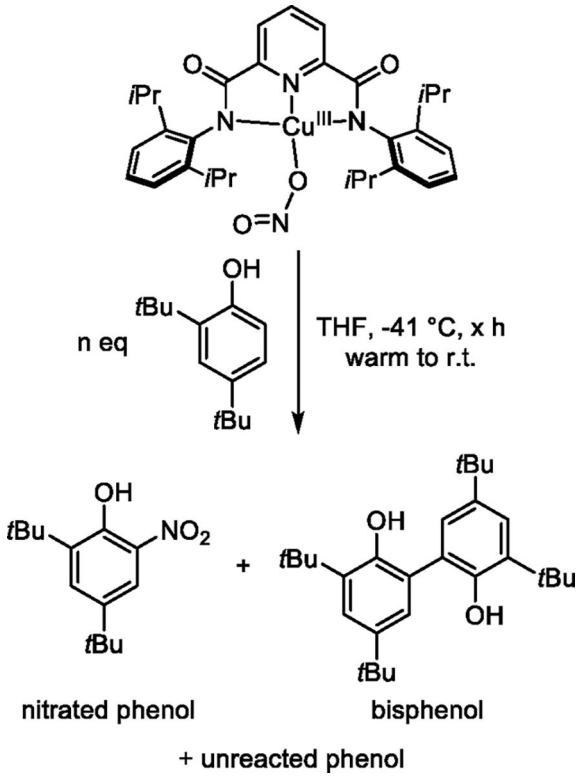

Scheme 2. Observed Reactants and Products When $LCuNO_2$ Is Reacted with DTBP

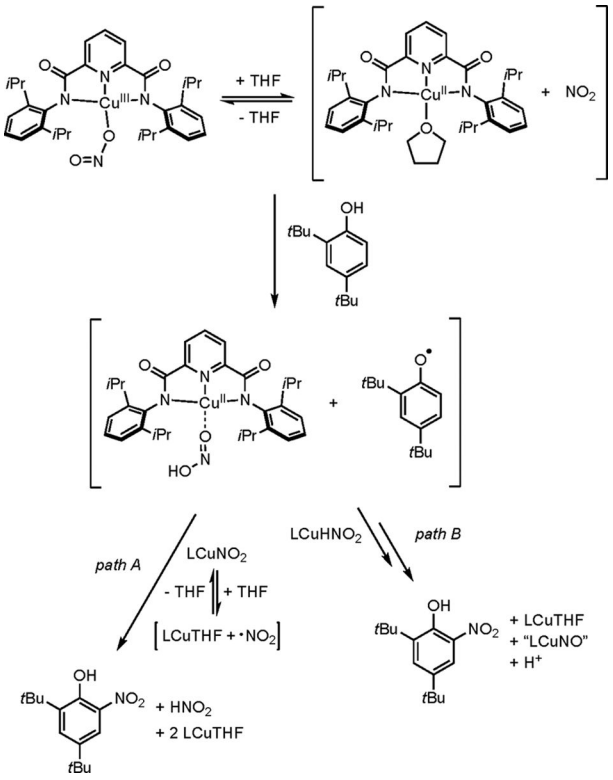

Scheme 3. Possible Mechanisms of Phenol Nitration by $LCuNO_2$

Table 1.

Results from Product Analysis of the Reactions between $LCuNO_2$ and Various Equivalents of DTBP[a]

equiv	nitrated phenol % yield	bisphenol % yield[b]	% of unreacted phenol	mass balance[c] (%)	% of phenol converted[d]
10	0.5	8.2	94	102.7	8.5
	0.7	8.8	95	104.5	9.1
1	15	42	45	102	56
	17	43	42	102	59
0.5	48	26	30	104	71
	46	24	28	98	71

[a]All data were from ^{1}H NMR spectral integrations using integration of the trimethoxybenzene peak at 6.09 ppm (3 protons) as a standard. All values are based on the DTBP loading.

[b]Values take into consideration that 2 mol of DTBP is required to form 1 mol of bisphenol.

[c]Mass balance values over 100% are due to the standard error in the ^{1}H NMR integration values.

[d]Calculated by the equation (nitrated phenol % yield + bisphenol % yield)/mass balance.